Article

Not peer-reviewed version

First Synthesis of Millimeter-Sized Single Crystals of High-Entropy Perovskite $(La_{0.25}Pr_{0.25}Sm_{0.25}Gd_{0.25})_{1-x}Ca_xMnO_3$ Oxides

Haiou Wang * and Haochen Wang

Posted Date: 12 May 2026

doi: 10.20944/preprints202605.0753.v1

Keywords: high-entropy oxide; single crystal growth; perovskite manganite; flux method; colossal magnetoresistance

 doi:10.20944/preprints202605.0753.v1

Article

First Synthesis of Millimeter-Sized Single Crystals of High-Entropy Perovskite $(La_{0.25}Pr_{0.25}Sm_{0.25}Gd_{0.25})_{1-x}Ca_xMnO_3$ Oxides

Haiou Wang * and Haochen Wang

Key Laboratory of Novel Materials for Sensor of Zhejiang Province, College of Materials and Environmental Engineering, Hangzhou Dianzi University, Hangzhou 310018, China

* Correspondence: wanghaiou@hdu.edu.cn

Abstract

We report the first successful synthesis of millimeter-sized single crystals of high-entropy perovskite manganites with the composition $(La_{0.25}Pr_{0.25}Sm_{0.25}Gd_{0.25})_{1-x}Ca_xMnO_3$ (x = 0.3, 0.4, 0.5). Single crystals exceeding 2 mm in size were grown via a flux method using a $PbF_2/PbO/B_2O_3$ system. The X-ray diffraction patterns exhibit only (0k0) series reflections, indicating strong preferred orientation and high-quality single-crystal character. Scanning electron microscopy reveals dense, grain-boundary-free surfaces. Energy-dispersive X-ray spectroscopy elemental mapping shows uniform distribution of all constituent elements without detectable segregation or secondary phases, confirming the formation of a true high-entropy solid solution in single-crystal form. To the best of our knowledge, based on the publicly searchable literature, this is the first report of bulk single-crystalline high-entropy perovskite oxide. This breakthrough provides a much-needed single crystal experimental platform for systematically investigating the intrinsic magnetotransport mechanisms of compositionally complex strongly correlated oxides, free from grain-boundary interference.

Keywords: high-entropy oxide; single crystal growth; perovskite manganite; flux method; colossal magnetoresistance

1. Introduction

Since formally defined by Rost et al. in 2015, high-entropy oxides have become a research frontier in functional materials [1]. These materials consist of five or more cations occupying the same crystallographic site in equimolar or near-equimolar proportions, stabilizing a single-phase solid solution through high configurational entropy, and exhibiting core effects such as high-entropy effect, sluggish diffusion, severe lattice distortion, and cocktail effect [1,2]. To date, high-entropy oxides have been successfully prepared in various structural types, including rock-salt [3], fluorite [4], perovskite [5], spinel [6], pyrochlore [7], and olivine [8], demonstrating rich functional properties in areas such as ionic conductivity, dielectricity, catalysis, magnetism, and energy storage [9–16].

Among the numerous high-entropy oxide systems, perovskite-type high-entropy manganites occupy a special position due to their unique physical implications. The B-site is occupied by Mn ions, and the continuous modulation of the Mn^{3+}/Mn^{4+} valence ratio can be achieved through A-site multi-element doping, thereby directly tuning the competition between double-exchange and superexchange interactions [17]. Variations in A-site ionic radii further modify the Mn–O–Mn bond angle and carrier bandwidth, providing multiple degrees of freedom for fine-tuning magnetoelectric properties [17]. It is this deep coupling between chemical complexity and strongly correlated electronic behavior that makes high-entropy manganite perovskites an ideal model system for exploring enhancement mechanisms of colossal magnetoresistance (CMR).

Indeed, significant progress has been made in engineering the magnetotransport properties of manganite perovskites using high-entropy design. Polycrystalline $(Gd_{0.25}La_{0.25}Nd_{0.25}Sm_{0.25})_{0.7}Sr_{0.3}MnO_3$

 doi:10.20944/preprints202605.0753.v1

prepared by Sarkar et al. via nebulized spray pyrolysis achieved a negative magnetoresistance exceeding 94% [18]; Mazza et al. demonstrated in $La(Cr_{0.2}Mn_{0.2}Fe_{0.2}Co_{0.2}Ni_{0.2})O_3$ thin films that compositionally disordered systems can maintain magnetic uniformity, and that the type of magnetic order and critical temperature can be continuously tuned [19]. These works indicate that the local potential fluctuations and strain distributions introduced by high-entropy disorder may provide a new route, distinct from conventional single-doping approaches, for enhancing CMR by amplifying the spatial inhomogeneity of exchange pathways and intensifying the competition between double-exchange and superexchange.

However, the aforementioned studies are all based on polycrystalline or thin-film samples. In polycrystalline systems, grain boundaries, pores, and local compositional fluctuations are inevitable. These microstructural features couple with the high-entropy disorder effects, producing significant extrinsic magnetoresistance contributions that make it difficult to separate intrinsic bulk mechanisms from extrinsic grain-boundary effects. Core physical issues such as phase competition, carrier localization, and magnetoresistance anisotropy are difficult to address conclusively in polycrystalline samples.

In contrast, single crystals, by eliminating grain-boundary scattering and orientational averaging effects, exhibit transport and magnetoresistance behavior closer to the intrinsic response of the material, and can directly reveal the directionality of exchange pathways and the anisotropy of magnetoresistance [20,21]. In the history of research on conventional CMR manganites, single-crystal experiments have always served as the gold standard for distinguishing bulk mechanisms from grain-boundary contributions and for validating theoretical models [20,21]. Therefore, the study of high-entropy manganite perovskites from polycrystals to single crystals is very important. However, single-crystal growth of multi-component high-entropy systems is extremely challenging. During prolonged high-temperature growth, multiple principal elements are highly susceptible to segregation, compositional mismatch, and oxygen stoichiometry deviations, leading to secondary phase precipitation or poor crystal quality. This technical bottleneck has resulted in a long-standing absence of bulk single crystals of high-entropy perovskite manganites, severely hindering the field's progression from phenomenological description to intrinsic mechanistic elucidation. Based on the publicly searchable literature, there is currently no report on bulk high-entropy single-crystal manganites.

This work breaks through the above bottleneck. Using a flux method, we have for the first time successfully prepared millimeter-sized large bulk high-entropy single crystals of $(La_{0.25}Pr_{0.25}Sm_{0.25}Gd_{0.25})_{1-x}Ca_xMnO_3$ (x = 0.3, 0.4, 0.5). Through X-ray diffraction, scanning electron microscopy, and energy-dispersive spectroscopy, we systematically characterized the crystal structure, morphology, and compositional uniformity, confirming that the obtained crystals possess high-quality single-crystal character and excellent high-entropy solid-solution homogeneity. This achievement fills the gap in the field of high-entropy manganite perovskite single crystals and provides an urgently needed experimental platform for systematically investigating the intrinsic modulation mechanism of disorder on CMR and related magnetoelectric properties, free from grain-boundary interference.

2. Experimental Methods

2.1. Crystal Growth

Single crystals of $(La_{0.25}Pr_{0.25}Sm_{0.25}Gd_{0.25})_{1-x}Ca_xMnO_3$ (x = 0.3, 0.4, 0.5) were grown by a high-temperature flux method. High-purity La_2O_3, Pr_6O_{11}, Sm_2O_3, Gd_2O_3, $CaCO_3$, and MnO_2 powders were mixed in stoichiometric ratios and combined with a $PbF_2/PbO/B_2O_3$ flux system in a mass ratio of 1:7 (precursor: flux). The flux composition was PbF_2: PbO: B_2O_3 = 0.8 : 0.195 : 0.005 by weight. The mixture was thoroughly ground in an agate mortar for 2–3 hours, transferred into a platinum crucible, and placed in a muffle furnace. The temperature was raised to 1250 °C at a rate of 200 °C/h, held for 48

 doi:10.20944/preprints202605.0753.v1

hours to ensure complete homogenization, then slowly cooled to 1000 °C at a rate of 0.5 °C/h, and finally naturally cooled to room temperature in the furnace.

2.2. Characterization

X-ray diffraction (XRD) patterns were collected using a diffractometer equipped with Cu Kα_1 radiation (λ = 0.15405 nm) over a 2θ range of 10–80° with a step size of 0.02°. Rietveld refinement was performed using the EXPGUI-GSAS software to obtain lattice parameters. Surface morphology was examined by scanning electron microscopy (SEM), and elemental composition and distribution were analyzed by energy-dispersive X-ray spectroscopy (EDS).

3. Results and Discussion

3.1. Crystal Structure

Figure 1 presents the XRD patterns, Rietveld refinement results, and corresponding photographs of the single crystals with x = 0.3, 0.4, and 0.5. The samples exhibit only three diffraction peaks, corresponding to the (020), (040), and (060) planes, indicating high orientation and good crystalline quality. Because the crystals grow preferentially along a specific crystallographic plane, the diffraction peaks of single-crystal samples are significantly reduced in number compared to the numerous peaks observed in polycrystalline samples, with regular angular intervals maintained between them. The main diffraction peak positions in Fig. 1 remain largely unchanged, indicating that the overall crystal structure does not undergo significant changes with varying Ca^{2+} doping levels. The photographs in the insets further show that the obtained crystals have relatively regular external morphology, well-defined facets, and dimensions all exceeding 2 mm, reflecting good single-crystal growth quality. The regular morphology and millimeter size attest to the high growth quality achieved by the flux method. Rietveld refinement was performed on ground crystal fragments. As shown in the refinement plots, the calculated patterns match well with the experimental data, and the low residual factors confirm that the samples are single-phase with an orthorhombic perovskite structure (space group *Pnma*).

 doi:10.20944/preprints202605.0753.v1

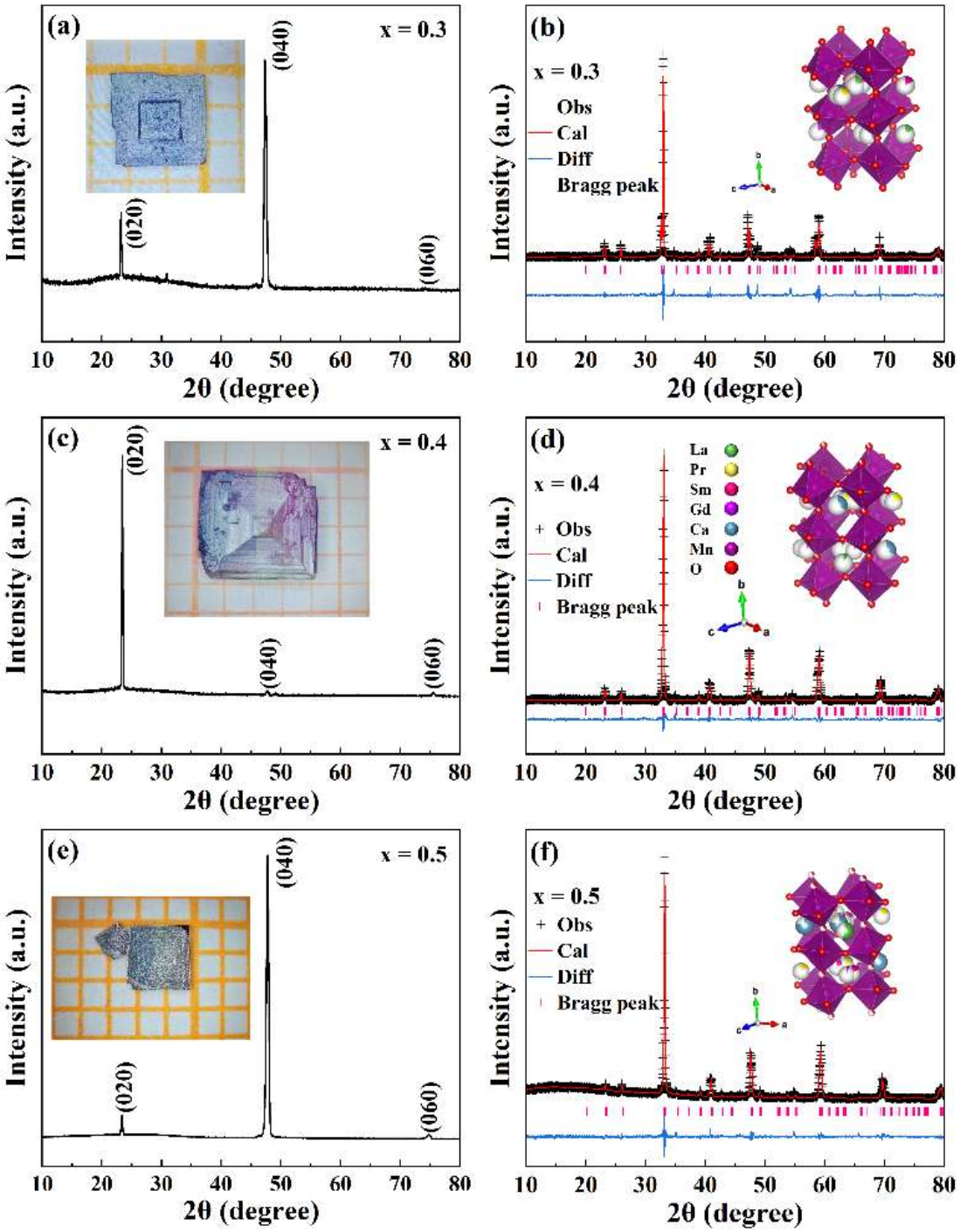

Figure 1. Photographs, room-temperature XRD patterns, and powders Rietveld refinement results of $(La_{0.25}Pr_{0.25}Sm_{0.25}Gd_{0.25})_{1-x}Ca_xMnO_3$ (x = 0.3, 0.4, 0.5) single crystals: (a)–(b) x = 0.3; (c)–(d) x = 0.4; (e)–(f) x = 0.5. The Rietveld refinement plots include calculated data (red solid line), observed data (black crosses), difference profile (blue line), and Bragg reflection positions (pink vertical bars). The inset shows a schematic of the crystal structure of $(La_{0.25}Pr_{0.25}Sm_{0.25}Gd_{0.25})_{1-x}Ca_xMnO_3$, illustrating the La/Pr/Sm/Gd/Ca ion doping and MnO_6 octahedra.

3.2. Surface Morphology

Figure 2 shows the surface micromorphology of the single crystals with x = 0.3, 0.4, and 0.5. The surfaces of all composition samples are generally dense, without the obvious grain-boundary features characteristic of polycrystalline samples. The absence of granular morphology, intergranular voids,

 doi:10.20944/preprints202605.0753.v1

and secondary phase inclusions serves as the key criterion for distinguishing single crystals from polycrystalline ceramics. Some step-like terraces and undulating features are visible on the crystal surfaces, which are associated with preferential faceted growth during the crystallization process and subsequent mechanical handling. The flux method employed in this work is capable of growing structurally integral, high-quality high-entropy perovskite manganite single crystals within a certain compositional range.

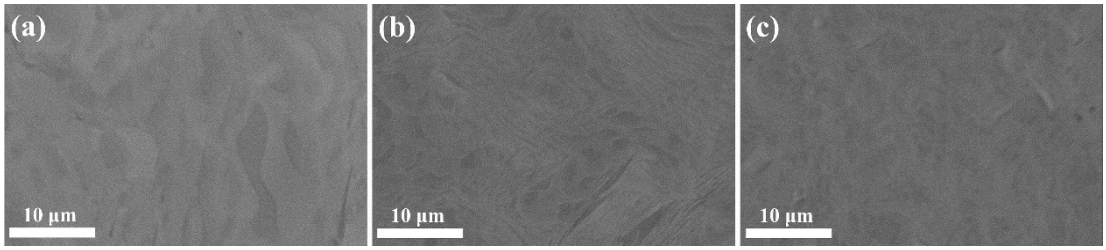

Figure 2. SEM images at 3000× magnification of $(La_{0.25}Pr_{0.25}Sm_{0.25}Gd_{0.25})_{1-x}Ca_xMnO_3$ (x = 0.3, 0.4, 0.5) single crystals: (a) x = 0.3; (b) x = 0.4; (c) x = 0.5.

3.3. Elemental Homogeneity

For a material to be classified as a high-entropy oxide, all constituent elements must be uniformly distributed within the detection limits of the characterization techniques, without compositional partitioning or secondary phase precipitation. Figure 3 presents the EDS elemental mapping results for single crystals with x = 0.3, 0.4, and 0.5. The elements La, Pr, Sm, Gd, Ca, Mn, and O are clearly detected across the surfaces of all three samples and are generally uniformly distributed, with no obvious large-scale elemental agglomeration or compositional separation observed. The uniform spatial distribution of the four rare-earth elements (La, Pr, Sm, Gd) together with Ca, Mn, and O provides direct evidence for the realization of a high-entropy solid solution in single-crystal form. The EDS results further indicate that the measured atomic ratios of the constituent elements are basically consistent with the nominal stoichiometric values, demonstrating the reliability of the flux method in preserving the target composition. This finding is significant. Elemental segregation during prolonged slow cooling represents one of the core challenges in high-entropy single-crystal growth. The successful suppression of segregation demonstrated in this work indicates that the $PbF_2/PbO/B_2O_3$ flux system provides a suitable chemical environment for maintaining multi-component homogeneity throughout the crystallization process.

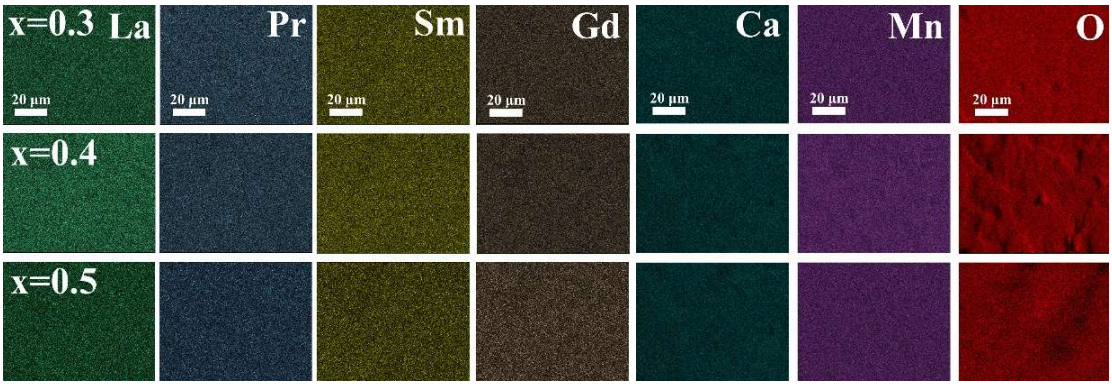

Figure 3. EDS elemental distribution maps of $(La_{0.25}Pr_{0.25}Sm_{0.25}Gd_{0.25})_{1-x}Ca_xMnO_3$ (x = 0.3, 0.4, 0.5) single crystals.

3.4. Comparison with Existing Literature

To clearly present the novelty of this work, Table 1 summarizes the representative high-entropy perovskite oxide systems reported in the literature, comparing their morphology and crystalline

 doi:10.20944/preprints202605.0753.v1

form. There are abundant reports on high-entropy oxides, with more than 20 references cited in this paper alone. However, all previous reports on high-entropy perovskite manganites have been limited to polycrystalline or thin-film forms. To the best of our knowledge, this work represents the first realization of bulk single-crystalline high-entropy perovskite oxide synthesis. This breakthrough transcends the barrier that has long confined the study of high-entropy manganites to grain-boundary-containing systems (such as polycrystals, thin films, and heterojunctions). The successful preparation of bulk single crystals of high-entropy perovskite manganites holds profound significance for the field of strongly correlated oxides.

For high-entropy systems, the interplay between chemical disorder and Jahn-Teller distortions is expected to generate complex physical landscapes, and directional measurements along specific crystallographic axes are irreplaceable for distinguishing the contributions of disorder-induced localization from conventional scattering mechanisms. Systematic investigations on the magnetism, transport properties, and magnetoresistance of these single crystals are in progress and will be reported elsewhere. The successful synthesis reported in this work represents the crucial first step toward a deeper and more rigorous understanding of disorder-tuned magnetism and magnetotransport mechanisms in high-entropy perovskite oxides.

Table 1. Comparison of morphology among representative high-entropy perovskite oxides in the literature.

System/Composition	Morphology	Crystallinity	Reference
$La(Cr_{0.2}Mn_{0.2}Fe_{0.2}Co_{0.2}Ni_{0.2})O_3$	Thin film	Polycrystalline	[19]
$(Gd_{0.25}La_{0.25}Nd_{0.25}Sm_{0.25})_{0.7}Sr_{0.3}MnO_3$	Ceramic	Polycrystalline	[18]
$Bi(Zn_{0.2}Mg_{0.2}Al_{0.2}Sn_{0.2}Zr_{0.2})O_3$-based	Ceramic	Polycrystalline	[22]
$Sr(Ti_{0.28}Zr_{0.18}Zn_{0.18}Sn_{0.18}Hf_{0.18})O_{3-\sigma}$	Ceramic	Polycrystalline	[23]
$(La_{0.25}Pr_{0.25}Sm_{0.25}Gd_{0.25})_{1-x}Ca_xMnO_3$	Bulk crystal	Single crystal	this work

4. Conclusions

Using a $PbF_2/PbO/B_2O_3$ flux method, we have for the first time successfully synthesized millimeter-sized high-entropy perovskite manganite single crystals of $(La_{0.25}Pr_{0.25}Sm_{0.25}Gd_{0.25})_{1-x}Ca_xMnO_3$ (x = 0.3, 0.4, 0.5). The cross-validation of three characterization techniques, XRD patterns showing only (0k0) series reflections, SEM observation of dense grain-boundary-free morphology, and EDS mapping of uniform elemental spatial distribution, provides conclusive evidence for the single-crystal nature and the formation of a high-entropy solid solution. This is the first report worldwide on bulk single crystals of high-entropy perovskite oxides. This achievement breaks through the long-standing technical bottleneck in high-entropy single-crystal growth and establishes a new experimental paradigm for systematically investigating the intrinsic physical behavior of compositionally complex strongly correlated oxides, free from the interference of grain boundaries and microstructural inhomogeneities.

 doi:10.20944/preprints202605.0753.v1

Author Contributions: Haiou Wang and Haochen Wang collected the experimental data; Haochen Wang participated in the material preparation and data analysis; Haiou Wang was the leader of the project, guiding experimental design, data collation, article writing and revision. All authors read and approved the final manuscript.

Data Availability Statement: All data are available from the corresponding author on reasonable request.

Acknowledgments: This research was supported by the National Natural Science Foundation of China (Nos. 11604067).

Conflicts of Interest: The authors declare no conflict of interest.

References

1. Rost C M, Sachet E, Borman T, et al. Entropy-stabilized oxides. Nature Communications, 2015, 6(1): 8485.
2. Schneider J M. How high is the entropy in high entropy ceramics?. Journal of Applied Physics, 2021, 130(15): 150903.
3. Su L, Ren J K, Lu T, et al. Deciphering structural origins of highly reversible lithium storage in high entropy oxides with in situ transmission electron microscopy. Advanced Materials, 2023, 35(19): 2205751.
4. Xu L, Su L, Niu M, et al. Irradiation induced structural damage and evolution of mechanical properties in high entropy fluorite oxide. Journal of the European Ceramic Society, 2023, 43(8): 3507-3515.
5. Chen L, Li B H, Guo J, et al. High-entropy perovskite $RETa_3O_9$ ceramics for high-temperature environmental/thermal barrier coatings. Journal of Advanced Ceramics, 2022, 11(4): 556-569.
6. Minouei H, Tsvetkov N, Kheradmandfard M, et al. Tuning the electrochemical performance of high-entropy oxide nanopowder for anode Li-ion storage via structural tailoring. Journal of Power Sources, 2022, 549: 232041.
7. Wright A J, Wang Q Y, Hu C Z, et al. Single-phase duodenary high-entropy fluorite/pyrochlore oxides with an order-disorder transition. Acta Materialia, 2021, 211: 116858.
8. Liu K, Zhang H W, Liu C, et al. Crystal structure and microwave dielectric properties of $(Mg_{i0.2}Zn_{0.2}Co_{0.2}Mn_{0.2})_2SiO_4$–A novel high-entropy ceramic. Ceramics International, 2022, 48(16): 23307-23313.
9. Jiao Y T, Dai J, Fan Z H, et al. Overview of high-entropy oxide ceramics. Materials Today, 2024, 77: 92-117.
10. Vinnik D A, Trofimov E A, Zhivulin V E, et al. High entropy oxide phases with perovskite structure. Nanomaterials, 2020, 10(2): 268.
11. Albedwawi S H, AlJaberi A, Haidemenopoulos G N, et al. High entropy oxides-exploring a paradigm of promising catalysts: a review. Materials and Design, 2021, 202: 109534.
12. Witte R, Sarkar A, Kruk R, et al. High-entropy oxides: an emerging prospect for magnetic rare-earth transition metal perovskites. Physical Review Materials, 2019, 3(3): 34406.
13. Zhao Z F, Chen H, Xiang H M, et al. High-entropy $(Y_{0.2}Nd_{0.2}Sm_{0.2}Eu_{0.2}Er_{0.2})AlO_3$: a promising thermal/environmental barrier material for oxide/oxide composites. Journal of Materials Science and Technology, 2020, 47: 45-51.
14. Okejiri F, Zhang Z H, Liu J X, et al. Room-temperature synthesis of high-entropy perovskite oxide nanoparticle catalysts through ultrasonication-based method. ChemSusChem, 2020, 13(1): 111-115.
15. Liu C J, Zhang D W, Li W, et al. Manganese-based A-site high-entropy perovskite oxide for solar thermochemical hydrogen production. Journal of Materials Chemistry A, 2024, 12(7): 3911-3922.
16. Huang C, Luo J, Mansley Z R, et al. Manganese-rich high entropy oxides for lithium-ion batteries: materials design approaches to address voltage fade. Journal of Materials Chemistry A, 2024, 12(38): 26253-26265.
17. Kumar A, Bérardan D, Dragoe D, et al. Magnetic and electrical properties of high-entropy rare-earth manganites. Materials Today Physics, 2023, 32: 101026.
18. Sarkar A, Wang D, Kante M V, et al. High entropy approach to engineer strongly correlated functionalities in manganites. Advanced Materials, 2023, 35(2): 2207436.
19. Mazza A R, Skoropata E, Sharma Y, et al. Designing magnetism in high entropy oxides. Advanced Science, 2022, 9(10): 2200391.

 doi:10.20944/preprints202605.0753.v1

20. Tomioka Y, Tokura Y. Bicritical features of the metal-insulator transition in bandwidth-controlled manganites: single crystals of $Pr_{1-x}(Ca_{1-y}Sr_y)_xMnO_3$. Physical Review B, 2002, 66(10): 104416.
21. Giot M, Beran P, Perez O, et al. $Bi_{1-x}Ca_xMnO_3$ (x = 0.4 and 0.45): X-ray single-crystal and electron microscopy study. Chemistry of Materials, 2006, 18(14): 3225-3236.
22. Zhou S Y, Pu Y P, Zhang X Q, et al. High energy density, temperature stable lead-free ceramics by introducing high entropy perovskite oxide. Chemical Engineering Journal, 2022, 427: 131684.
23. Liu Y F, Hou J D, Cheng C F, et al. The effect of non-equimolar doping on the preparation and electrical conductivity of Sr(Ti, Zr, Zn, Sn, Hf)$O_{3-\sigma}$ high entropy perovskite oxide. Ceramics International, 2023, 49(13): 21546-21554.